

Optimising the wave attenuation of bamboo fences using the numerical wave model SWASH

Marijn Alferink¹, Alejandra Gijon Mancheno¹, Tomohiro Suzuki², and Ad Reniers¹

Abstract

Mangroves protect tropical coastlines from flooding and erosion, reducing flood risks along coastal communities worldwide. Nevertheless, mangrove forests have experienced considerable losses due to activities like urbanization and aquaculture, exposing coastal areas to wave attack. To restore mangroves at eroding coastlines, structures formed by bamboo poles and a brushwood filling are used to shelter the coast from waves, and create a favourable habitat for mangrove colonization. However, these structures often lose their brushwood filling during storms, resulting in high maintenance costs. This study proposes a new type of design to reduce maintenance expenses, consisting of only vertical bamboo poles without a filling of brushwood. Structure designs are evaluated for a case study in Demak, Indonesia, using the numerical wave model SWASH to predict wave attenuation through the structures. Field measurements and WaveWatch III data are analyzed to obtain the design conditions for the structures in Demak. SWASH is validated against laboratory experiments, and applied to investigate the optimum number of rows and their optimum spacing (in the direction of wave propagation). The model shows that for a structure consisting of two rows of bamboo poles, the transmission rate E_t/E_i decreases from 75% to 55% when the row spacing in the wave direction is increased from $s_x = 0.42$ m to $s_x = 5.8$ m. Larger spacings do not result in less transmission, and at least three rows are needed to have a transmission rate lower than 50 % - a common wave reduction target used in restoration efforts with structures. This study thus identifies potential strategies to maximize wave attenuation by bamboo structures, which can be used to reduce wave attack along muddy coasts without the need of a brushwood filling. Hereby, it provides an economically and user friendly alternative with respect to the previous brushwood structure designs, as it requires less material costs and maintenance. In addition, this study presents a new method to schematize these kind of structures in SWASH in an efficient way.

Keywords:


SWASH, Nature Based Solutions, Wave Attenuation, Mangroves

¹m.alferink@tudelft.nl,
A.GijonMancheno-1@tudelft.nl,
A.J.H.M.Reniers@tudelft.nl; Delft University of
 Technology, Delft, The Netherlands
²tomohiro.suzuki@mow.vlaanderen.be; Flanders
 Hydraulic Research, Antwerp, Belgium

This paper was submitted on 12-07-2022. It was accepted after double-blind review on 20-06-2023 and published online on 25-09-2023.

DOI: <https://doi.org/10.48438/jchs.2023.0027>

Cite as: “Alferink, M., Gijon Mancheno, A., Suzuki, T., Reniers, A.J.H.M., Optimising the wave attenuation of bamboo fences using the numerical wave model SWASH. Journal of Coastal and Hydraulic Structures, 3, p.27, <https://doi.org/10.48438/jchs.2023.0027>”

The Journal of Coastal and Hydraulic Structures is a community-based, free, and open access journal for the dissemination of high-quality knowledge on the engineering science of coastal and hydraulic structures. This paper has been written and reviewed with care. However, the authors and the journal do not accept any liability which might arise from use of its contents. Copyright © 2023 by the authors. This journal paper is published under a CC BY 4.0 license, which allows anyone to redistribute, mix and adapt, as long as credit is given to the authors. 

1 Introduction

Mangroves are intertidal ecosystems, usually found in the tropics between 5 °N and 5 °S, where they grow naturally at coastlines and deltas (The United Nations, 2003). Mangrove forests provide several ecosystem services such as coastal protection, food and timber provision, among many other functions (Barbier et al., 2011), which makes them a very valuable environment for coastal communities.

The coastal defence function of mangroves relates to their ability to attenuate waves (Quartel et al., 2007; Massel et al., 1999; Bao, 2011) and trap sediment between their roots (McIvor et al., 2013). Therefore, mangrove forests mitigate coastal erosion and protect the hinterland from flooding. However, in several countries around the world, mangrove areas were transformed into fish ponds over the 20th century. As mangroves were removed, the natural protection that they provide was also lost, resulting in higher exposure to wave action and erosion.

Over the past decades the restoration of mangrove ecosystems has received increasing attention in many countries in South-East Asia (Schmitt et al., 2013; Winterwerp et al., 2020; Albers et al., 2013; Tonneijck et al., 2015). This paper focuses on the coastline of Demak, in North Java, Indonesia, which was largely deforested and transformed into rice fields and aquaculture ponds. Extensive groundwater extraction in the nearby city of Semarang also causes high subsidence rates in the area, reaching up to 16 cm/year (Abidin et al., 2013; Hamilton and Casey, 2016). The rising water levels combined with the higher wave exposure due to mangrove loss have caused coastline retreat rates of several hundreds of meters per year (Winterwerp et al., 2020).

Mangrove establishment is hindered at coastlines exposed to wave action and erosion, as mangrove seedlings require windows of opportunity with low hydrodynamic conditions to settle and survive (Balke et al., 2011; Rees, 2019). In order to reduce wave action and mitigate erosion in Demak, permeable structures made out of bamboo poles and a brushwood filling were built in shallow waters between 2014-2020, approximately 100 m away from the coast (Tonneijck et al., 2022). These structures aimed to cause sufficient wave attenuation to stop coastline retreat, creating a sedimentation area where mangroves can establish.

Over the course of the project, the structures required frequent maintenance as their filling easily degraded due to wave action. A follow up project (MuMaCo) therefore implemented new designs that aimed to reduce maintenance costs, consisting of row(s) of vertical orientated poles without a brushwood filling. The structures were built in a pilot study in 2021, and were formed by bamboo poles with a diameter of $D = 0.12-0.15$ m, a lateral spacing of $s_y = 0.18$ m (perpendicular to the waves), and a separation of $s_x = 4.5$ m between poles (in the wave direction). Nevertheless, these pilot designs were based on engineering judgement, since design tools for anisotropic structures formed by cylinders were lacking at the time of their implementation.

The design requirements for the structures can be divided in the following stages:

1. Initially structures need to attenuate waves, to create a sheltered environment where sediment can deposit. Sedimentation behind the structures is a function of the wave attenuation they produce, and the local morphodynamic conditions. Over time, seedlings can colonise the newly created land.
2. The hinterlying basin should be accessible by drifting seedlings, meaning that the existing coastline should be directly connected to the newly accreted land.
3. The designs should prevent the settled seedlings from being torn loose by erosion or wave action.
4. The designs should continue to prevent erosion over time, which requires designs that adapt to changing morphodynamic conditions.
5. The basin created behind the structures should drain properly to ensure that the deposited sediment strengthens over time.

This study focuses on the first requirement, i.e. on developing tools to predict wave attenuation by anisotropic structures formed by bamboo poles (without brushwood). Existing studies in the mangrove restoration literature have mainly investigated the hydrodynamic performance of brushwood structures. For instance, a field measurement campaign carried out in Vietnam monitored wave transformation through structures that successfully created sedimentation basins near the coast (Albers et al., 2013). The measurements of Mai Van et al. (2021) of a 1:1 model of a brushwood structure show similar results as that of Albers et al. (2013), with 30 - 60 cm of sedimentation in 10 months in 2016 at Mekong deltaic coasts in Vietnam.

The flow through homogeneous cylinder fields has also been thoroughly studied to understand the effect of emergent vegetation on wave and currents (Dalrymple et al., 1984; Nepf, 1999; Maza, 2019). Dalrymple et al. (1984) developed a model to predict wave transmission through a homogeneous and highly permeable vegetation field, assuming negligible wave reflection by the cylinders and considering that they have a negligible effect on the local velocity field. However, although the bamboo poles of the structures considered here are cylindrical, they most likely violate the assumptions of Dalrymple et al. (1984), as the bamboo poles have very small spacings in the lateral direction.

Experimental studies suggest that rows of cylinders with lateral spacings below $s_y = 1.5D$, where D is the diameter of the bamboo pole, have a significant effect on the surrounding flow by contracting the flow into a jet and also causing

reflection (Bonakdar et al., 2015). Note that the existing structures in Demak have even smaller lateral separations, down to 1.25 times the pole diameter ($D = 0.15$ m).

Modelling of wave propagation through vegetation and coastal structures has received increasing attention over the last decade and many hydrodynamic models have been improved and extended with vegetation modules. The theories of Mendez and Losada (2004) and Dalrymple et al. (1984) have been widely used to implement vegetation in various numerical models, where Mendez and Losada (2004) is an extension of Dalrymple et al. (1984) to include irregular waves, in phase-averaging wave models like SWAN (Suzuki et al., 2012; Chen and Zhao, 2012). Whereas in more extensive phase-solving models, like among others XBeach and SWASH, (van Rooijen et al., 2016; Cao et al., 2015; Suzuki et al., 2019; Yin et al., 2021) the dissipation by vegetation is based on the Morison Equation (Morison et al., 1950).

The numerical model SWASH has been successfully applied to model wave propagation through vegetation fields and through coastal structures at nearshore areas, and it has been validated against data collected in laboratory studies (Phan Khanh, 2019; Suzuki et al., 2019). Brushwood structures have also been modelled in SWASH by Dao (2018); Dao et al. (2021); Mai et al. (2020). However, previous studies focused on homogeneous cylinder arrangements and on structures filled with a brushwood filling under regular or mild wave conditions (Dao et al., 2021). In contrast, the bamboo fences in this study are not homogeneous, nor are they filled with a brushwood filling, and they are also exposed to storm conditions which could occur in their lifetime (of 2-5 years).

This research thus investigates how to model structures formed by (multiple) rows of bamboo poles using the vegetation module of SWASH, and explores the structure performance under storm conditions for several potential bamboo structure configurations. The model performance is validated using laboratory measurements by Jansen (2019), and applied to quantify wave reduction and identify strategies to maximize wave attenuation by a bamboo structure. This study thus provides valuable steps towards the efficient implementation of bamboo structures to promote mangrove restoration.

The topic of the paper is introduced in Section 1. Section 2 contains the methodology, which describes the model SWASH, the validation and design scenarios. The model results of different design scenarios are presented in Section 3. The implications of these results for the morphodynamic evolution are discussed in Section 4. In Section 5 the conclusions of this paper are presented.

2 Methods

2.1 Structure design conditions

The coastline of Demak is located in North Java (Indonesia), and it is bordered by the city of Semarang in the South ($-6^{\circ}94'00.44''$ N, $110^{\circ}42'37.76''$ E) and by the Wulan river delta in the North ($-6^{\circ}75'81.34''$ N, $110^{\circ}54'90.44''$ E). The local wave climate is characterized by two monsoon seasons. During the North-Western (NW) monsoon (November-February) offshore waves with a significant wave height of $H_{m0} = 2$ m and a significant wave period of $T_s = 6$ have been observed, whereas during the South-Eastern (SE) monsoon (March-October) mild wave conditions prevail, with $H_{m0} = 0.3$ m and $T_s = 3$ s (Van Domburg et al., 2018). The tide in Demak is mixed, mainly diurnal with a form factor of 1.72, a tidal spring range of 85 cm and a neap tidal range of 50 cm (Tas et al., 2020).

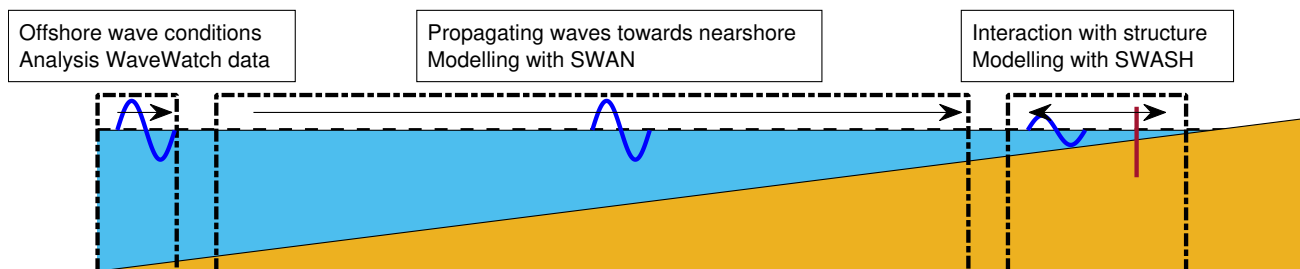


Figure 1: Overview of used models, near the structures the waves are modelled with SWASH.

During the NW monsoon, storms are the main facilitator in sediment transport towards the coast in Demak (Ton-

neijck et al., 2015; Winterwerp et al., 2005). However, storms also cause erosion at the coast (van Bijsterveldt et al., 2022). Most studies investigating the performance of structures for mangrove restoration report mild wave conditions, or provide wave datasets that are too short to derive design conditions for return periods longer than a year. Here a WaveWatch III data set spanning 12.5 years was used to determine the local offshore design wave conditions with a General Pareto Distribution. The design conditions with a 1 year and 5 year return period were then propagated to the nearshore area with the model SWAN. Note that the offshore wave condition analysis and the simulations with SWAN are not a part of this paper, but can be found in Alferink (2022). Closer to shore, SWASH is applied to model wave propagation through the structures, see Figure 1.

Wave attenuation targets for the structures are obtained from the monitoring study of Albers et al. (2013). Their study investigated stiff brushwood structures that caused 17 centimeters of accretion after 7 months. These sedimentation rates were obtained with transmission coefficients of $K_t = 0.7-0.8$ when the structures were submerged (during high water levels), and $K_t = 0.5-0.6$ when they were emerged (during low water levels), where the transmission rate K_t is defined as $K_t = H_t/H_i$, with H_t and H_i being the transmitted and incoming wave height, respectively. In terms of energy these wave transmission rates corresponds with energy transmission rates of $E_t/E_i = 50-64\%$ for submerged cases and $25-36\%$ for emerged cases. The measurements of Mai Van et al. (2021) of a 1:1 model of a brushwood structure show similar results as that of Albers et al. (2013), with 30-60 cm of sedimentation in 10 months in 2016 in Mekong deltaic coasts in Vietnam. These accretion rates were obtained using structures with transmission rates ranging between $K_t = 0.7-0.9$ for submerged cases and $K_t = 0.55-0.7$ for emerged cases, or in terms of energy $E_t/E_i = 50-80\%$ and $30-50\%$, respectively. The highest waves considered in the study by Mai Van et al. (2021) are slightly smaller than the wave conditions with a return period of 1 year in this study.

2.2 SWASH

SWASH is a numerical model that can simulate non-hydrostatic, free-surface, rotational and transport flow phenomena in one, two, or three dimensions (SWASH Manual). Here the model is used in a two-dimensional profile mode using multiple layers. The corresponding model governing equations are the continuity equation (Equation 1) and the non-hydrostatic shallow water equations in the cross-shore (Equation 2) and vertical direction (Equation 3):

$$\frac{\partial \zeta}{\partial t} + \frac{1}{\partial x} \int_{-d}^{\zeta} u dz = 0 \quad (1)$$

$$\frac{\partial u}{\partial t} + u \frac{\partial u}{\partial x} + u \frac{\partial w}{\partial z} + g \frac{\partial \zeta}{\partial x} + \frac{\partial q}{\partial x} = -\frac{1}{\rho} F_x \quad (2)$$

$$\frac{\partial w}{\partial t} + w \frac{\partial u}{\partial x} + w \frac{\partial w}{\partial z} + \frac{\partial q}{\partial z} = -\frac{1}{\rho} F_z \quad (3)$$

here ζ is the surface elevation [m], h is the water depth [m], t is the time [s], z is the location in the vertical [m], u is the flow velocity in the x (cross-shore) direction [m/s], w is the flow velocity in the z (vertical) direction [m/s], x is the location on the horizontal plane [m], z is the location in the vertical plane [m], g is the gravitational constant [m/s²], q is the non-hydrostatic pressure, F_x and F_z present body and surface forces in x and z direction [N].

The bamboo structures are implemented in SWASH with the use of the vegetation module, where the bamboo poles and the metal cylinders of the laboratory experiments are schematized as rigid plant stems. The vegetation module requires input for following parameters: number of stems or cylinders per m², N_{stems} , diameter of the cylinders D [m], the drag coefficient C_d [-], and the height of the cylinders h_v [m]. The cylinders are assumed to be evenly spread out over the vegetation patch. SWASH calculates the volumetric flow acceleration through a homogeneous volume of cylinders (Figure 2,b) but does not resolve the individual cylinders, nor the associated cross-sectional flow acceleration between poles (Figure 2,a) or the wakes behind the poles, which are accounted for through the drag coefficient. This approach allows to describe the structure/vegetation in a 2D profile mode (x and z only) assuming lateral uniformity.

For vertical cylinders only the horizontal force component F_x is introduced in the non-hydrostatic shallow water equations, under the assumption that the horizontal loads acting on a cylinder are much larger than the horizontal skin friction forces. The expression of F_x is given by the Morison equation (Morison et al., 1950):

$$F_x = \frac{1}{2} \rho C_d D u |u| + \rho C_M A \frac{\partial u}{\partial t} \quad (4)$$

where ρ is the density of water in [kg/m³], C_d is the drag coefficient [-], D is the diameter of the cylinder [m], $C_M = C_m + 1$ [-], is the inertia coefficient, C_m is the added mass coefficient [-], A is the cross-sectional area of the cylinder ($\pi D^2/4$) [m²], and $\frac{\partial u}{\partial t}$ is the flow acceleration in [m/s²].

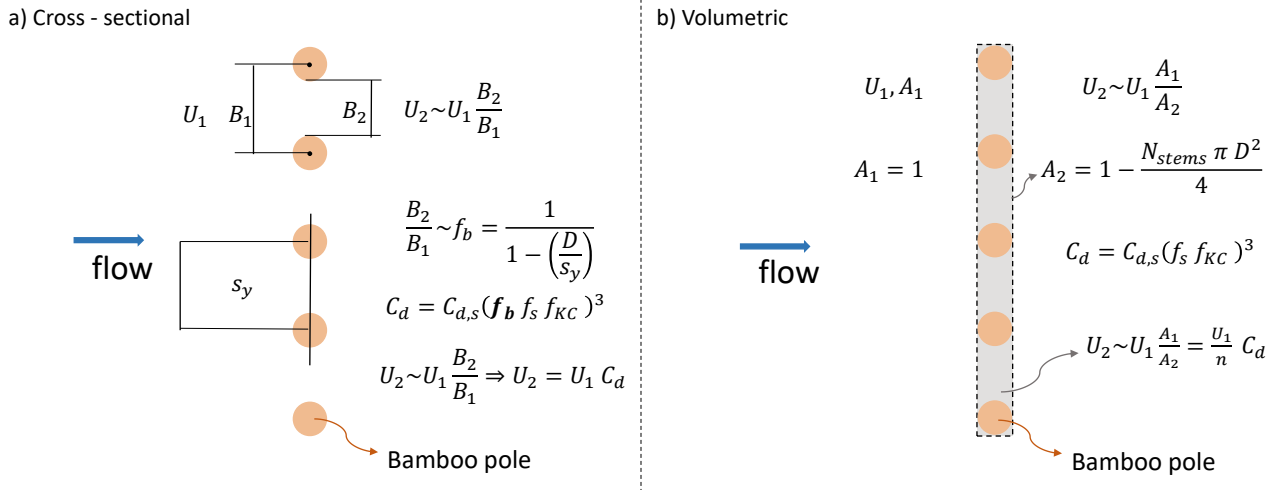


Figure 2: Top view of the mass conservation schematizations. a) The cross sectional method is characterised by a reduction in the flow cross-section (B_2/B_1) between the cylinders, which is expressed in the blockage factor, see Equation 11. b) The volumetric method is characterised by the reduction in fluid volume (or in the bottom area A_2/A_1 assuming a constant water level) between cylinders, which is expressed in the porosity n

The effect of the bamboo poles on their surrounding flow, and thus on the drag force component, is often parameterized using a bulk drag coefficient, $C_{d,b}$ [-], resulting in:

$$F_{x,drag} = \frac{1}{2} C_{d,b} D u_\infty |u_\infty| \rho_w \quad (5)$$

where u_∞ [m/s] is the undisturbed flow velocity upstream from the structure, and where changes of velocity through the bamboo poles are therefore included in $C_{d,b}$. Here the bulk drag coefficient is calculated using the empirical expressions of Gijon Mancheno et al. (2021), which derive $C_{d,b}$ as the product of the drag coefficient of a single cylinder, $C_{d,s}$, times a characteristic velocity factor:

$$C_{d,b} = C_{d,s} \left(\frac{u_c}{u_\infty} \right)^3 \quad (6)$$

The characteristic flow velocity u_c represents how the velocity changes through a group of cylinders, and it is given by three empirical coefficients:

$$u_c = u_\infty f_{kc} f_s f_b \quad (7)$$

where f_b , f_s and f_{KC} are factors that account for the processes of blockage (Etminan et al., 2019), sheltering and the flow regime expressed by the KC number (Keulegan and Carpenter, 1958). KC is defined as:

$$KC = \frac{u_\infty D}{T} \quad (8)$$

where T is the wave period [s]. The factor f_{KC} represents the transition region between inertia and drag-dominated conditions, according to:

$$f_{KC} = 0.012KC + 0.44 \quad (9)$$

Sheltering by the wakes of upstream cylinders is calculated according to:

$$f_s = 1 - \frac{c_s}{s_x/D} \quad (10)$$

where c_s is an empirical coefficient dependent on the turbulent intensity, s_x is the center-to-center distance between two adjacent cylinders in the flow direction. Gijon Mancheno et al. (2021) obtained a value of $c_s = 0.796$ by fitting their model to force measurements inside cylinder arrays.

Flow acceleration due to flow contraction through a cross-section of cylinders, also denoted as blockage, is modelled based on mass conservation through a cross-section of the structure, resulting in:

$$f_b = \frac{1}{1 - D/s_y} \quad (11)$$

where s_y is the lateral distance between two adjacent cylinders (perpendicular to the flow direction), center-to-center, in m. The blockage factor f_b was introduced by Etminan et al. (2019) and van Rooijen et al. (2020), who found that the effect of flow contraction between cylinders on the drag forces is better represented by the reduction in cross-section rather than by the volume reduction inside a cylinder field.

The volumetric approach is implemented in the momentum equations in SWASH, and can be activated and deactivated in the model simulations. When this approach is used, the volumetric porosity of the structure is defined as $n = A_c/A = 1 - N_{stems}0.25\pi D^2$ (see Figure 2,b) and every velocity term in the shallow water equations is divided by n . The u -momentum equation, Equation 2, therefore becomes the following when the porosity module is activated:

$$(1 + C_m(1 - n)) \frac{\partial(\frac{u}{n})}{\partial t} + n \frac{\partial(\frac{u}{n})^2}{\partial x} + \frac{\partial w \frac{u}{n}}{\partial z} + n(g \frac{\partial \zeta}{\partial x} + \frac{\partial q}{\partial x}) + \frac{1}{2} C_D \frac{h_v}{h} N_{stems} \frac{u}{n} \left| \frac{u}{n} \right| D = 0 \quad (12)$$

where u [m/s] is the flow velocity at each layer in SWASH and the drag force acting on the cylinders includes a submergence factor dependent on the ratio of the submerged height of the cylinders within a layer h_v [m] to the layer thickness h [m], the cylinder density per unit area N_{stems} [cylinders/m²] and the diameter of poles D [m]. The corresponding drag coefficient is defined using Equation 7.

In case of a volumetric approach, the blockage factor f_b is set to one as flow acceleration affects are accounted for by the porosity. The drag force term in Equation 12 then becomes:

$$\frac{1}{2} \mathbf{C}_{d,s}(\mathbf{f}_s \mathbf{f}_{KC})^3 \frac{h_v}{h} N_{stems} \frac{u}{n} \left| \frac{u}{n} \right| b_v \quad (13)$$

where the differences with the original term are indicated by the bold font.

The second option is a cross-sectional approach (see panel a in Figure 2). In this case the porosity is not included in the momentum equations. Instead, the original equations are used (Equations 1-3) and blocking is incorporated in the drag force term by the blockage factor f_b in Equation 7, resulting in:

$$\frac{1}{2} \mathbf{C}_{d,s}(\mathbf{f}_s \mathbf{f}_b \mathbf{f}_{KC})^3 \frac{h_v}{h} N_{stems} u \left| \frac{u}{n} \right| b_v \quad (14)$$

2.3 Validation case

For the validation of SWASH, the model performance is compared with the experiments of Jansen (2019), which measured the reduction of regular waves by different arrays of cylinders in the wave flume of the Delft University of Technology. Two different structure configurations are selected: a single row of cylinders perpendicular to the wave direction (referred as single row) and a configuration formed by several rows of cylinders (denoted as longitudinal configuration). The wave conditions consist out of 6 cases where the wave height is kept constant at $H = 0.13$ m and the wave period (T) varies between 1 and 3 seconds, see Table 1. The poles are emerged at all times and the still water depth is 55 cm. The diameter of the individual cylinders is 4 cm. For more information, see Jansen (2019).

A 2DV (x and z) grid with a grid size $dx = 3$ cm is used for all the wave conditions, providing 50 datapoints for the shortest wave, which corresponds with the minimum number of points required by SWASH (see SWASH manual). The number of vertical layers is dependent on the wave number, and for the shorter and steeper waves, more layers are needed to have stable runs (SWASH manual). Thus, 3 equidistant layers are used for the shorter waves, and 2 layers for wave periods longer than $T = 1.25$ s.

Table 1: Wave conditions used in experiments by Jansen (2019)

T	H	d	L	k	c	n	c_g	kd	N_{Ursell}	KC
[s]	[m]	[m]	[m]	[1/m]	[m/s]	[-]	[m/s]	[-]	[-]	[-]
1	0.13	0.55	1.53	4.11	1.53	0.55	0.84	2.26	1.82	10.43
1.25	0.13	0.55	2.23	2.82	1.78	0.64	1.14	1.55	3.89	11.17
1.5	0.13	0.55	2.92	2.15	1.94	0.72	1.40	1.18	6.66	12.32
1.75	0.13	0.55	3.57	1.76	2.04	0.79	1.60	0.97	9.96	13.65
2	0.13	0.55	4.22	1.49	2.11	0.83	1.75	0.82	13.91	15.13
3	0.13	0.55	6.68	0.94	2.23	0.92	2.05	0.52	34.87	21.46

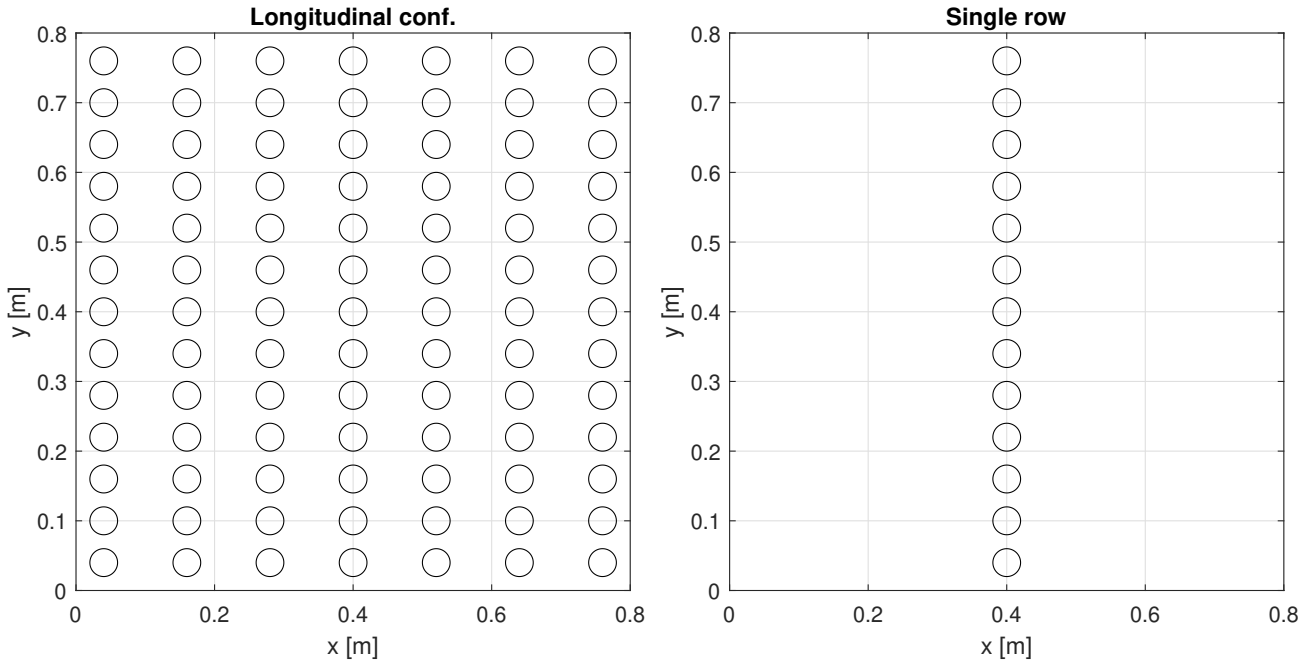


Figure 3: Top view of the structure configurations of Jansen (2019), which can also be found in Gijon Mancheno et al. (2021). The measurements of wave attenuation through these structures are used to test the performance of SWASH for a) a structure formed by several rows of cylinders and b) a single row of cylinders.

Important choices in schematizing the configurations of Jansen (2019) in SWASH are: the assumption of uniform placement of the poles, the approach to calculate the drag coefficient, the cylinder density N_{stems} and the way to describe mass conservation in Equation 2. Several alternatives are analyzed to define each of these processes in SWASH. To choose the drag coefficient, model simulations are compared using a bulk drag coefficient as defined by Gijon Mancheno et al. (2021) (Equation 6) with simulation results using the drag coefficient of a single cylinder, equal to $C_{d,s} = 2$ for the range of KC tested in the experiments (Sumer and Fredsoe, 2006). To define the density of (bamboo) poles, two approaches are compared: the first method defines the number of poles as the average value over the (seafloor) area covered by the structures, and the second method defines the individual rows of the structure (see Figure 4). To define mass conservation, we compare the cross-sectional and volumetric approach (Figure 2). Lastly, the possibility to bypass the assumption of uniform placement is studied, as this enables to design non-uniform structures. In Table 4 there is an overview of all the runs that have been used in the validation study. The row width and the density are equal in runs 7 and 8, but the underlying grid is different.

Table 2: Drag coefficient for the longitudinal configuration for the two different mass conservation methods: Volumetric and Cross-sectional.

T [s]	1	1.25	1.5	1.75	2	3
Volumetric $C_{d,b} = C_{d,s}(f_s f_{KC})^3$	0.14	0.15	0.16	0.17	0.17	0.17
Cross sectional $C_{d,b} = C_{d,s}(f_b f_s f_{KC})^3$	3.87	4.05	4.35	4.71	5.14	7.27

Table 3: Drag coefficient for the single row configuration for the two different mass conservation methods: Volumetric and Cross-sectional. The drag coefficients of $T = 2$ and 3 s are capped off, as they would be otherwise unrealistic high.

T [s]	1	1.25	1.5	1.75	2	3
Volumetric $C_{d,b} = C_{d,s}(f_{KC})^3$	0.35	0.37	0.41	0.43	0.43	0.43
Cross sectional $C_{d,b} = C_{d,s}(f_b f_{KC})^3$	9.48	10.0	11.59	11.66	11.66	11.66

For the simulation of the laboratory conditions, SWASH provides water level files that are processed with a script of the Hydraulic laboratory of the TU Delft using the method of Goda and Suzuki (1976) to separate the incoming,

Table 4: Overview of the numerical experiments for the validation study.

Run	Configuration	Mass conservation	Block or row by row	dx	Characteristics	N_{stems}
1	Single row	volumetric approach		3 cm		278
2	Single row	cross sectional approach		3 cm		278
3	Longitudinal	volumetric approach	row by row	3 cm		278
4	Longitudinal	cross-sectional approach	row by row	3 cm		278
5	Longitudinal	cross-sectional approach	block	3 cm		154
6	Longitudinal	cross-sectional approach	block	3 cm	$C_{d,s}$ instead of $C_{d,b}$	154
7	Longitudinal	cross-sectional approach	row by row	2 cm		287
8	Single row	volumetric approach		2 cm		287

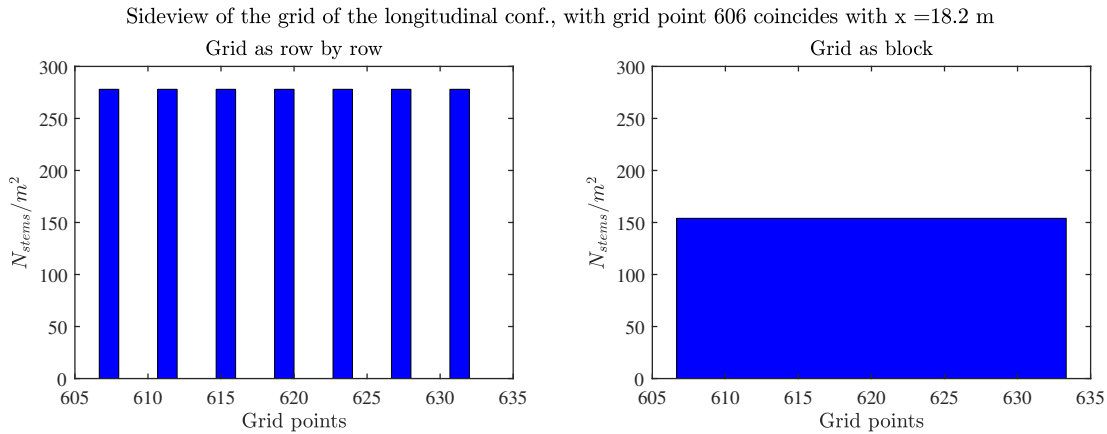


Figure 4: Sideview of the implementation of the poles in SWASH, with on the left) a row by row defined grid and on the right) the poles are equally distributed over the area as block instead of separate blocks(rows). The total amount of poles is in both options the same.

reflected and transmitted wave heights. With the use of the energy balance (Equation 15) the wave dissipation can be determined:

$$E_i = E_t + E_d + E_r \tag{15}$$

where E_i is the energy of the incident waves, E_t is the transmitted wave energy, E_d is the dissipated wave energy and E_r is the energy of the reflected waves.

2.4 Design setup

The offshore waves are implemented in SWASH by means of a weakly reflective boundary condition using Fenton (1988) theory to generate the non-linear waves with 10 higher harmonics, in order to describe the waves accurately. A 2D (z and x) setup with a grid size dx of 5 cm is used and a timestep which is controlled by the CFL condition, with a maximum and minimum Courant number of 0.5 and 0.2, respectively. Note that a larger grid size in the design phase is used than in the validation phase as the considered wave periods are longer (see Table 5). For the design waves two layers over the vertical are used to have a better representation of the velocity profile, as for these type of waves the depth averaged flow velocity is an overestimation of the real flow velocity (Suzuki et al., 2019)

Three wave conditions are modelled to capture the range of wave conditions expected in the field. The waves that are used are regular waves. The first one describes the daily wave conditions that are present in Demak throughout most of the year, which is based on measurements from Tas et al. (2020). As a second condition, a wave condition with a return period of 1 year is considered to be representative to study the transmission target through the structures. Thirdly, for the most extreme wave conditions, a return period of 5 years is used as the structures have a lifetime of approximately 2-5 years, and the H_{max} is determined using Battjes and Groenendijk (2000), for which the $H_{0.1\%} = H_{0.1\%}$ is chosen. A more elaborate description of the wave conditions is provided by Alferink (2022).

Table 5: Nearshore design wave conditions and parameters at depths varying between 0.8 and 1.9 m. KC and Re are determined using the maximum orbital velocity using linear wave theory for regular waves.

Condition	R	H	T_p	surge	tide	d	L	N_{Ur}	KC	Re
	[years]	[m]	[s]	[m]	[m]	[m]	[m]	[-]	[-]	[-]
Daily		$H_{m0} = 0.25$	3	0	0	0.8	7.9	30.5	10.0	$4.90 * 10^4$
Transmission	1	$H_{m0} = 0.80$	6.88	0.63	0.35	1.78	29	111	47.3	$1.01 * 10^5$
Extreme	5	$H_{max} = 1.32$	7.47	0.68	0.425	1.91	32	189	81.7	$1.61 * 10^5$

To obtain the transmission rates induced by the structures in the field, the method of Dekkers (2018) is used to process the outcomes from SWASH since the waves are non-linear. This method is an extension of Hughes (1993) and is first described in Guza and Thornton (1980). Note that a different method is used to process the wave simulations of laboratory experiments and the field design as the field conditions are much more non-linear (see Table 5) and the method of Goda and Suzuki (1976) is not able to process them accurately.

The drag forces are calculated with the Morison Equation (Equation 4) at the location of the first row of poles of the design, since these give the highest forces. The maximum drag force during a wave period, under regular waves, is used to characterize each design case. The drag forces are calculated at the still waterline for the emergent designs (daily wave conditions and $R = 1$ year) and for the submerged designs the forces are calculated at the top of the poles ($d = 1.78$ m). The drag force is multiplied with the water depth, assuming uniform flow as the structures are in shallow waters.

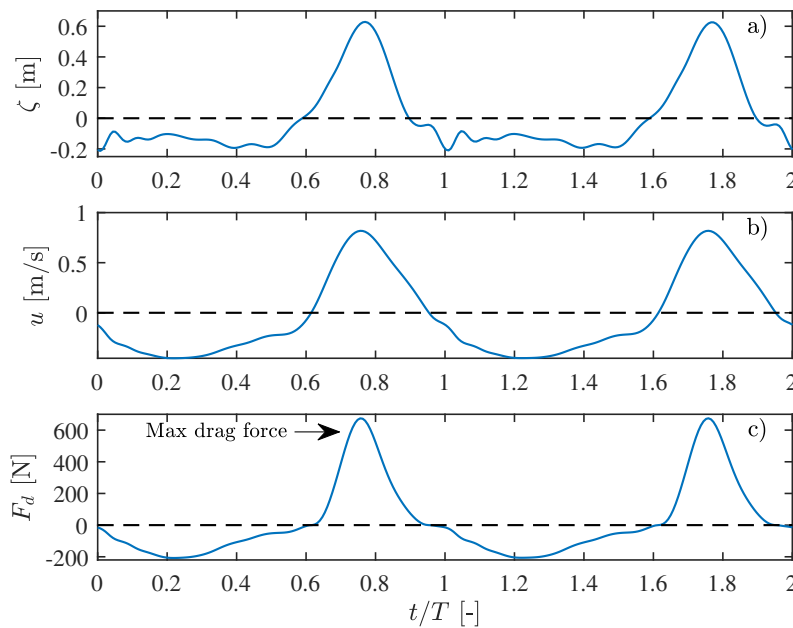


Figure 5: Drag force calculation for a design condition with a return period of 1 year and structure with three rows, with a row to row distance of $s_x = 5.8$ m. With a) water elevation with respect to still water depth, b) flow velocity at the still water depth and c) the drag force. The maximum drag force is used as characteristic value.

Three types of designs are considered: single row, double row and extended row, see Figure 6. The single row consists of a single row of bamboo poles, this design enables to study the interaction of waves with an unsheltered structure. The bamboo poles are placed with a lateral distance of $s_y = 1.5D = 0.21$ m.

The double row design consists of two rows of bamboo poles placed with a variable distance s_x between rows. This design enables to study the effect of the row spacing on wave propagation through the structure, and whether a resonance pattern could be induced between two rows of poles to generate extra dissipation. The extended row design consists of two to seven rows of bamboo poles. This design enables to study the effect of multiple rows with a fixed row spacing on wave transmission.

Table 6: General parameters of the designs.

Design	D	s_x	s_y	n	poles height	N_{stems}
units	m	-	-	-	m	poles/m ²
Single row	0.14	-	1.5 D	44.5 %	1.78	25
Double row	0.14	3 D to L_1	1.5 D	44.5 %	1.78	25
Extended row	0.14	$L/5$	1.5 D	44.5 %	1.78	25

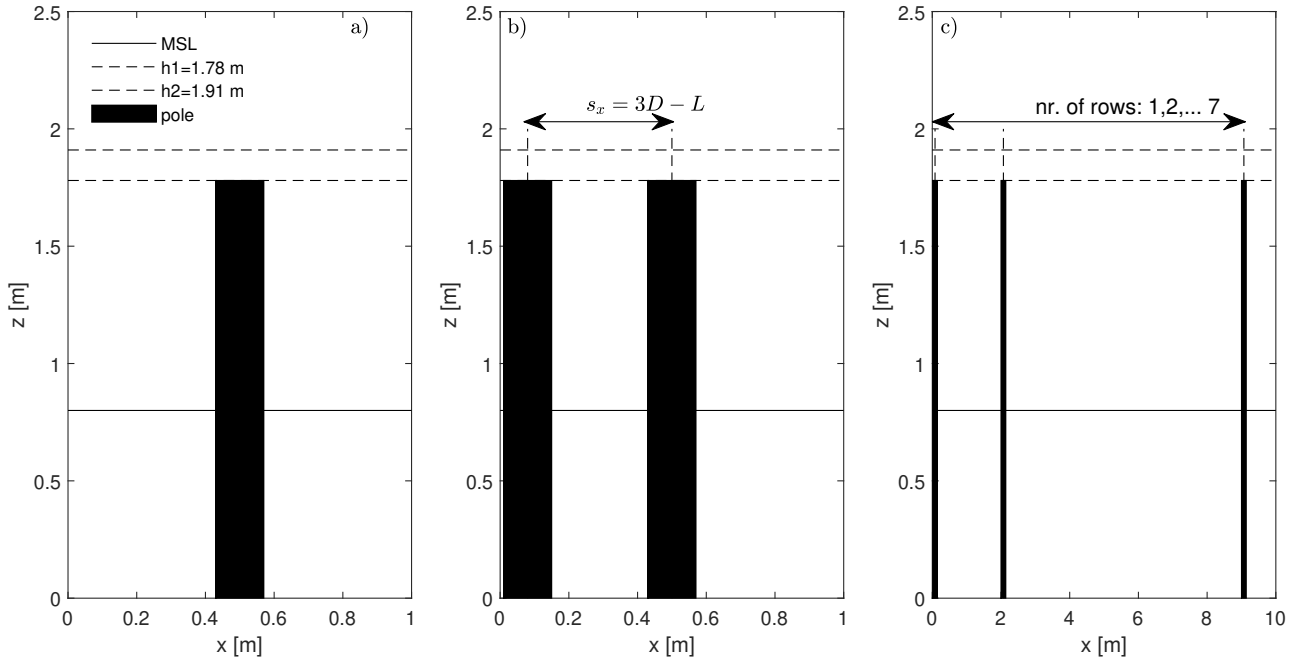


Figure 6: From left to right the sideviews of: the single row (a), double row (b) and extended row (c) designs. S_x is defined between the center lines of the poles.

3 Results

3.1 Validation wave transformation with SWASH

To implement the configurations studied by Jansen (2019) in the vegetation module in SWASH, four parameters are studied: the number of (bamboo) poles, the drag coefficient, the way to describe the mass conservation, and the assumption of uniform placement of cylinders.

The choice of drag coefficient is studied in Figure 7, where the simulation results obtained using the bulk drag coefficient from Gijon Mancheno et al. (2021) are inter-compared with simulation results using the drag coefficient of a single cylinder. As can be observed in Figure 7, using the bulk drag coefficient $C_{d,b}$ provides a better agreement with the measurements.

The different definitions of the bamboo pole density (per row, or using an average value for the whole structure) show minimal differences (see Figure 8). Thirdly, the different approaches to describe mass conservation inside the structure (see Section 2) are compared in Figures 9 and 10.

The results of the simulations with a single row configuration are shown in Figure 9. It can be seen that the transmission measurement has a better agreement with the volumetric approach, while the reflection shows a good agreement with both methods. For the dissipation rates, the cross-sectional approach gives too high values, in contrast with the volumetric approach that provides dissipation rates that are generally too low with a minimum for $T = 2$ s. The result of the SWASH simulations with the longitudinal configuration are shown in Figure 10. It can be observed that in this case the cross-sectional approach provides good agreement for the transmission and the dissipation rates, whereas the volumetric approach produces insufficient dissipation, and thus does not match well with the measurements. The reflection rates are reasonably well-reproduced with both approaches.

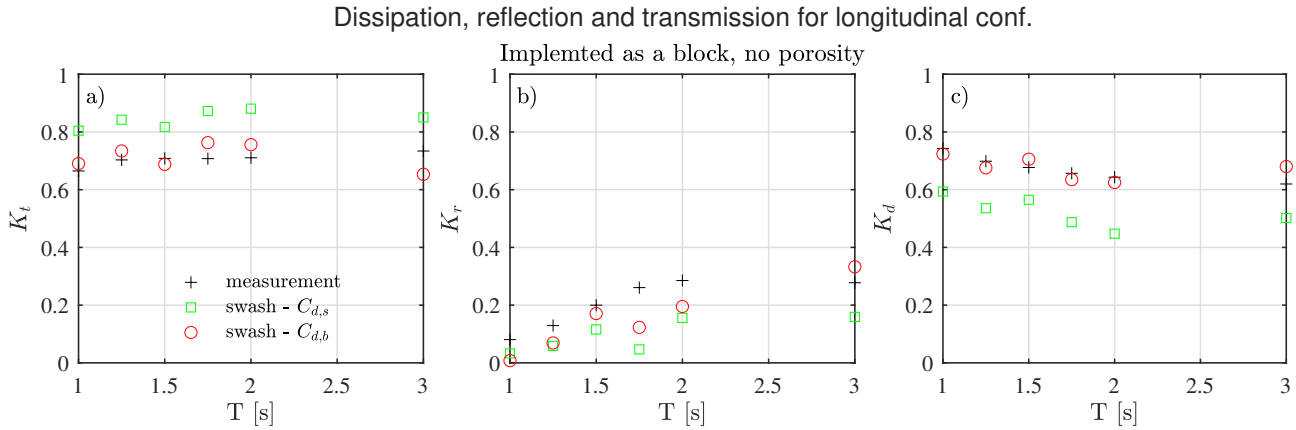


Figure 7: Comparison of the wave transformation using the bulk drag coefficient ($C_{d,b}$, red circle) compared with a drag coefficient of a single cylinder ($C_{d,s}$, green square) with observations (+ signs). With from left to right: a) transmission b) reflection and c) dissipation.

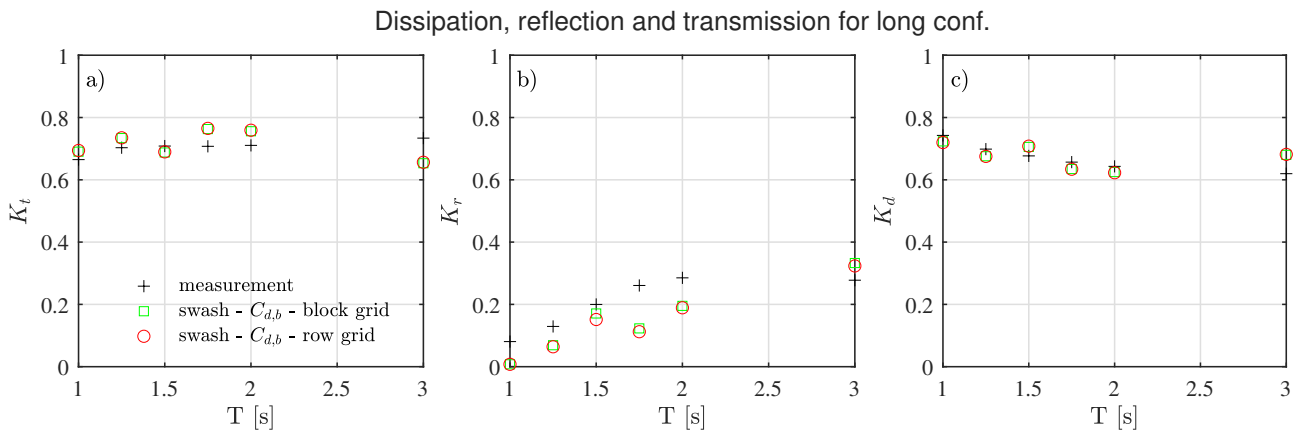


Figure 8: The results of defining the grid of poles with two different options for the longitudinal configuration. With from left to right: a) transmission b) reflection and c) dissipation. The differences between the two methods are small.

These results show the best overall match with the measurements, which is obtained with the cross-sectional approach, and is therefore used to implement designs with multiple rows in SWASH. Contrary to what was observed at the single row configuration in Figure 9, a different mass conservation method gives better results for the longitudinal configuration. This suggests that there is not one straightforward method that suits all cases. For the assumption of uniform placement of poles see Appendix A.

3.2 Design evaluation

The first design modelled in SWASH is the single row. For this configuration, the volumetric approach has been used to describe mass conservation in SWASH, and the corresponding drag coefficients can be found in Table 3. Note that the drag coefficient of the daily wave conditions is slightly larger than for more extreme conditions, since $C_{d,s} = 2$ for $KC = 10$, whereas for $R = 1$ and 5 years $C_{d,s} = 1.4$, as for these wave conditions (with $KC = 47.3$ and 81.7, respectively) the drag coefficient of a single cylinder $C_{d,s}$ is unaffected by the KC state and it is therefore asymptotic around this value (Sumer and Fredsoe, 2006). As result, $C_{d,b} = 0.35, 0.31$ and 0.31 for the daily conditions, 1-year return period, and 5-year return period, respectively.

The results for the three wave conditions (daily conditions, and storm conditions with return periods of 1 and 5 years) are presented in Table 7. It can be seen that all the transmission rates exceed 82%, thus not reaching the desired transmission rate of 50%. More dissipation is therefore needed to obtain designs that induce sufficient accretion.

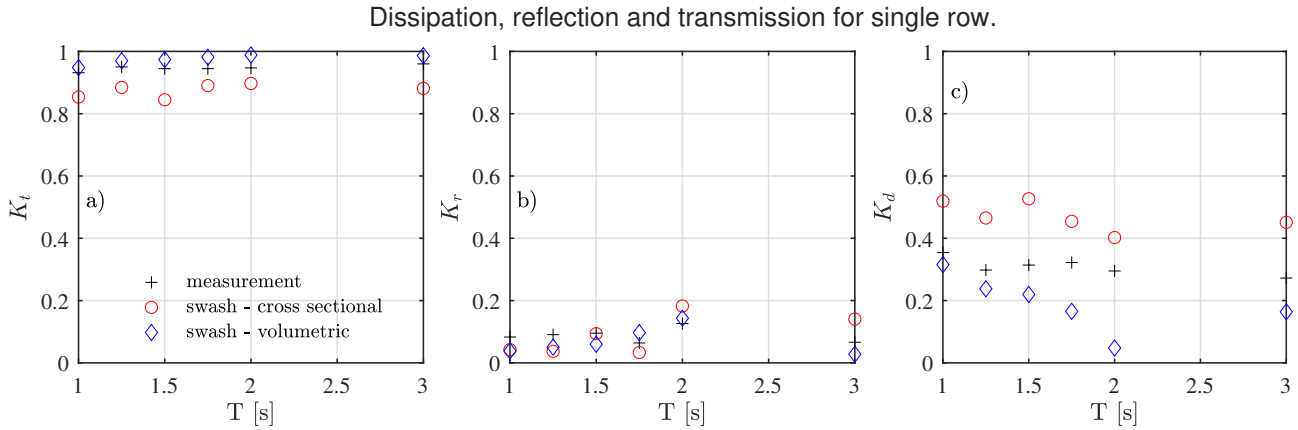


Figure 9: Validation of the single row configuration from Jansen (2019) (shown in Figure 3) for (from left to right): wave transmission, reflection, and dissipation as a ratio to the incoming wave, i.e.: $K_{t,r,d} = H_{t,r,d}/H_i$. The x-axis shows the wave period, belonging to the wave conditions indicated in Table 1.

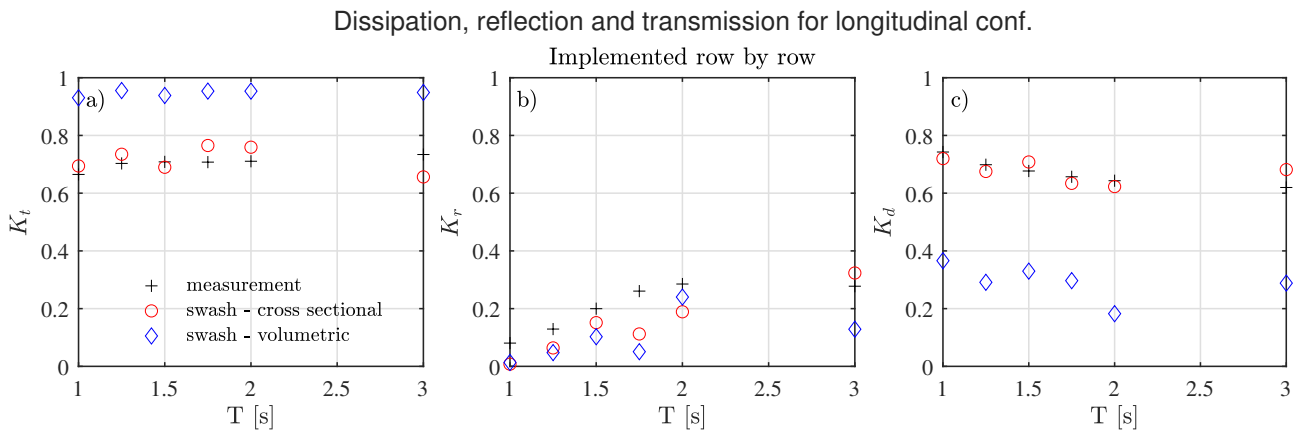


Figure 10: Validation of the longitudinal configuration from Jansen (2019); Gijon Mancheno et al. (2021), see Figure 3, with from left to right: transmission, reflection and dissipation in the form of $K_{t,r,d} = H_{t,r,d}/H_i$. On the x-axis are the wave periods belonging to the wave conditions in Table 1.

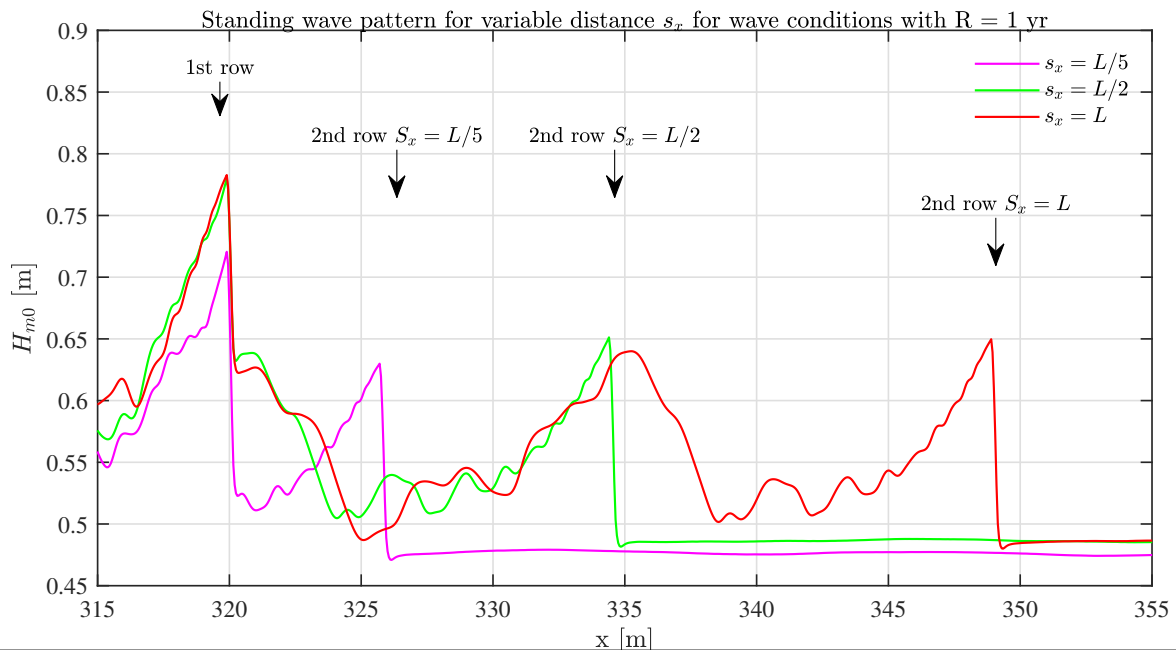


Table 7: Results single row design, with from left to right: transmission, reflection, dissipation and drag forces. All transmission rates are higher than the required rate of 50 %

Wave conditions	E_t/E_i	E_r/E_i	E_d/E_i	F_d (N)
Daily	0.82	0.028	0.15	3.7
R = 1 years	0.85	0.014	0.1	30
R = 5 years	0.93	0.01	0.06	72.6

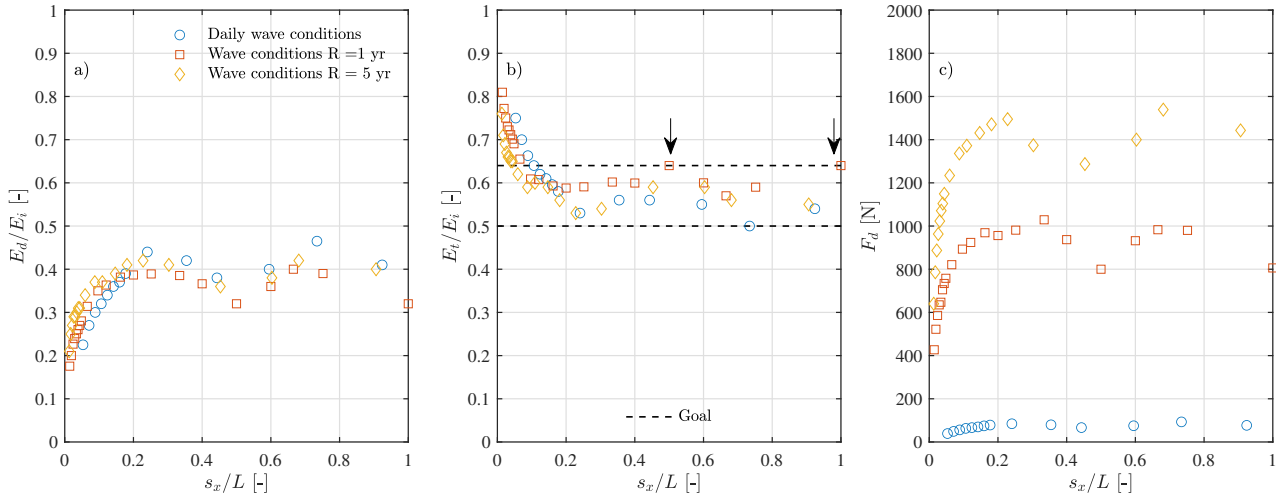


Figure 11: Results of wave interaction with double row design, see Figure 6(b & e), with from left to right: dissipation, transmission and drag forces. The dissipation and transmission rate is in the form of $E_{r,t}/E_i = H_{r,t}^2/H_i^2$. On the x-axis is the relative distance of the two rows, as function of the wave length of the wave condition

Next, the use of two rows of bamboo poles is examined by varying the separation in wave direction (with only incident waves), see Table 8 in Appendix B for the row separation and drag coefficient values. Figure 11 (b) shows that the transmission rates increase with larger separation between rows up to $s_x = L/5$, where the results seem to stabilize around a value of 55% for all wave conditions. After this point there are a few outliers at $s_x = (0.5-1)L$, for which the transmission rates are higher and the forces (Figure 11 c) are significantly lower. Moreover, an increase in the transmission rates of the daily wave conditions can be also observed just before $s_x = L_0/2 = 7.9$ m, corresponding to a distance that gives the same outliers for the higher wave conditions, $s_x = L_1/2$ and $L_5/2$. The reflection rates for this design are low, and remain below 6% (see Figure 18 in Appendix C).

With the help of Figure 12, the outliers (see arrows of Figure 11) are studied more in detail. In Figure 12 the significant wave height H_{m0} is shown as a function of the cross-shore distance x between rows for three configurations, consisting of 2 rows with a cross-shore separation of $s_x = L/5, L/2$ and L , respectively. The first row can be easily identified at $x = 320$ m. The second fences are at $x = 326$ m for the first configuration ($s_x = L/5$), at $x = 335$ m for the second ($s_x = L/2$), and at $x = 350$ m for the third ($s_x = L$). It can be observed that for $s_x = L/2$ & L , the wave height at $x = 320$ m is 5 cm higher than for $s_x = L/5$. This location corresponds with an anti-node, present at a distance of $L/2$ seawards (to the left) from the second row according to theory (Holthuijsen, 2007), therefore these do not occur for $s_x = L/5$ but only for the other two as can be observed in the figure. The nodes that should occur at $x = L/4$ or $3/4L$ are less clear due to the presence of the higher harmonics. Due to the anti-node at the first row, the horizontal velocities acting on the structure also become smaller, reducing wave dissipation and increasing wave transmission through the structure (Figure 11 b and c). At the same time the drag forces are also smaller for these particular row to row distances, as the drag force is calculated by means of the Morison Equation, in which the horizontal flow velocity is used (see Equation 4).

The effect of multiple rows of poles on the wave dissipation is studied with the extended row design. In order to do so, a constant distance of $s_x = 5.8m = L_1/5$ is used between rows, which is the optimal separation for which longer separations do not lead to more dissipation. In Figure 13 it can be observed that at least three rows are needed to reach the wave transmission goal of 50%. Next to this, it is shown that the effect of adding an extra new row to the design becomes less effective with an increasing amount of rows, fitting the theory of an asymptotic decline of the wave height by Dalrymple (1988). Besides this, the drag forces in Figure 13 c) are stable, indicating that the forces

are not increased due to internal wave reflection.

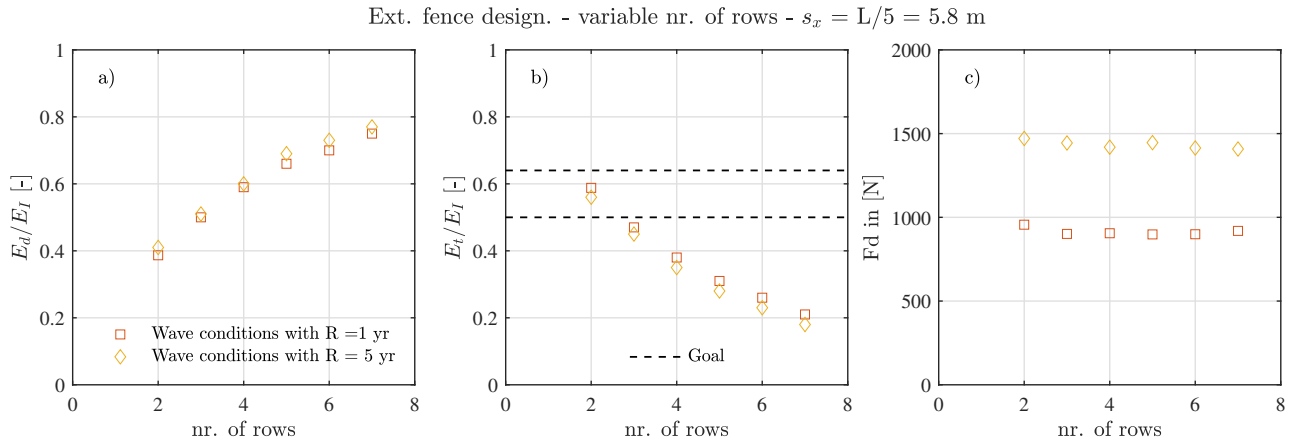


Figure 13: Result of the extended row design, with from left to right: transmission, dissipation and drag forces on the first row. The dissipation and transmission rate is in the form of $E_{r,t}/E_i = H_{r,t}^2/H_i^2$. On the x axis is the number of rows, with a constant row distance of $s_x = 5.8\text{m} = L_1/5$

4 Discussion

4.1 Uncertainties in sedimentation behind structures

This manuscript investigates wave propagation by structures that aim to mitigate erosion. In order to reflect on the potential effect the designs can have on the sediment transport, the shear stresses in front and behind the double row design are estimated for the three wave conditions modelled in the previous section. The following formula (Swart, 1976) is used to calculate the wave-driven shear stresses:

$$f_w = \left(-6 + 5.2 \left(\frac{u_w}{2.5d_{n50} \frac{2\pi}{T_s}} \right)^{0.19} \right) \quad (16)$$

$$\tau = \frac{1}{2} \rho_w f_w |u_w| u_w \quad (17)$$

The shear stress is calculated with the following parameters, $d_{n50} = 710^{-6}$ [m], $\rho_w = 1025$ [kg/m³] and using (maximum) the bottom velocities underneath the crest of the waves.

Based on the absolute shear stresses (see Figure 14 a), a structure causes a reduction in shear stress but no sedimentation is expected since $\tau > \tau_c = 0.017$ N/m² (Gijon Mancheno, 2022), where $\tau_c = 0.017$ N/m² is the critical shear stress for erosion in Demak. However, fully preventing erosion during these strong storm events may not be necessary as causing net accretion over the year may be enough for mangrove establishment (assuming that mangroves can grow long-enough roots during calmer conditions). On the other hand, based on the relative shear stress shown in Figure 14 (b), a reduction of more than 60% of the shear stress is observed due to the presence of the structures, which could potentially lead to sedimentation. However, this should be verified by measurements of the pilot study mentioned in Section 1.

Although the measurement campaign of Albers et al. (2013) provides wave reduction rates that were associated with accretion, they only spanned a period of 7-8 months and the long term effect of the structures that they investigated is therefore unknown. The 4-year long monitoring study done by Deltares in Demak showed that brushwood structures caused on average 0.3 m of accretion after their first NW season, and almost negligible sedimentation afterwards. Nevertheless, this area was heavily sinking, and since the subsidence rates were not quantified locally, it is difficult to extract conclusions about the net effect of the structures on the bed level. Smaller water depths behind the structure would reduce the wave energy even more, providing conditions that favour sedimentation. However since the sediment is mainly brought in by the incoming tide, which could be deflected by the structures, the sediment may not reach the hinterlying basin (Winterwerp et al., 2020).

Absolute and relative shear rate for designs with 3 rows and $s_x = L/5$

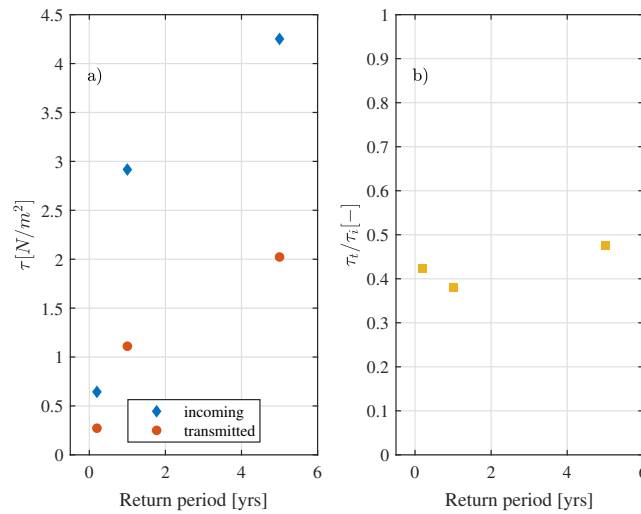


Figure 14: a) shear stress and b) shear rate reduction over the designs with on the x-axis the three wave conditions, R (Return period) = daily, 1 and 5 years. The shear stress may seem large but these are quite extreme conditions, and with 3 rows of bamboo poles there is a reduction of around 60 % of the shear stresses.

A significant way of sediment transport that is identified for the muddy coast of Guyana (Winterwerp et al., 2020) is the wave-driven streaming of mud, which is hypothesised to occur as well in Demak (Winterwerp et al., 2020; Borsje, 2019) and could be blocked by permeable structures (Borsje, 2018). With the structures built in Demak between 2014-2020, this was solved by leaving gaps between structures so that the sediment-laden flow could enter the basins. The openings also facilitate the drainage of the basin (Winterwerp et al., 2020), drying and strengthening the newly deposited sediment. The designs proposed in this study are more open and may not need these gaps, but it is yet unsure how they would interact with sediment transport due to mud-streaming.

4.2 Limitations of the bulk drag parametrization

The model of Gijon Mancheno et al. (2021), used to determine the $C_{d,b}$, includes a factor that describes a relation between the bulk drag coefficient and the KC number (f_{KC}). However, the choice of C_d for a single cylinder also depends on the KC number. The KC -dependency may thus be incorporated twice (and be overestimated) in drag force predictions.

The sheltering factor f_s was given values that were fitted in the experiments of Jansen (2019), nevertheless, in this study it is used outside its calibration range. Since field waves are higher and longer than in the laboratory experiments, Re values in Demak range between 1-1.6 10^5 , whereas in the laboratory they remained within 6.7-11.9 10^3 . It is thus expected that the turbulent intensity will be higher in the field, and that wakes will therefore be longer than in the experiments, producing lower bulk drag coefficients. A lower bulk drag coefficient would in turn cause lower wave dissipation rates and increase wave transmission.

The center to center distance s_y (perpendicular to the waves) was kept constant in this study, since the experiments of Jansen (2019) did not test values smaller than $s_y = 1.5D$. Smaller lateral spaces could lead to high reflection rates, and higher flow acceleration around the structures. The optimal lateral spacing should thus be investigated in future studies.

In the validation results the cross-sectional method shows the best agreement with the measurements for the longitudinal configuration, but for the single row configuration the volumetric has better results. This implies that different approaches could reproduce the same results, so this should be evaluated in future studies concerning the vegetation module in SWASH.

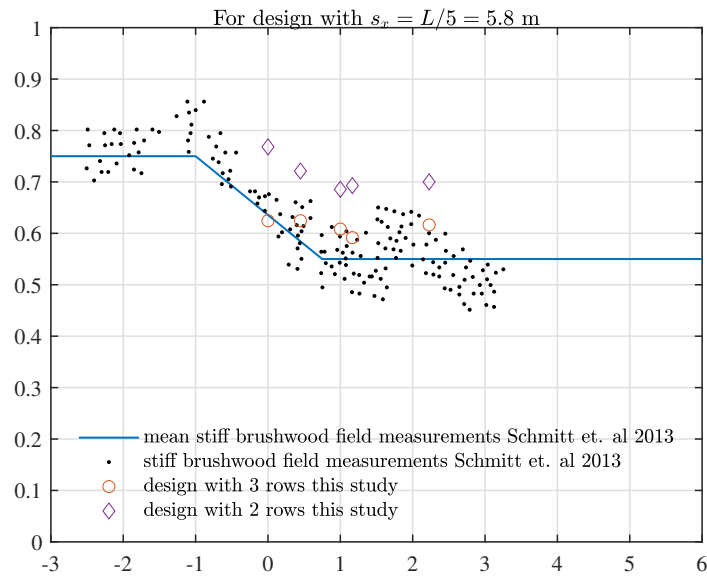


Figure 15: In order to compare the transmission rates $K_t = H_t/H_i$ is used.

4.3 Influence of varying water level

The water depth is not a constant value in the field, as varies with tides and surges. Therefore, the influence of the water depth on the wave transmission rate is studied using five different depths ranging from the design water level ($d = 1.8$ m) to mean sea level ($d = 0.8$ m). The wave heights are a function of the water depth, $H = 0.55d$ and they are given a constant wave period of $T = 6.88$ s. The wave attenuation performance of structures for different water levels is compared with measurements of Albers et al. (2013).

It can be observed in Figure 15 that wave transmission rates follow the same trend as the measurements of Schmitt et al. (2013) for the water levels where the structure is emerged (right side of Figure 15), suggesting that the relation between relative free board and transmission could be independent of the type of structure.

Figure 15 also indicates that at least 3 rows of bamboo poles are needed to reduce the wave energy behind the structure to 55% for the design water level ($R_c/H_i = 0$).

5 Conclusions

This study investigates the optimisation of bamboo structure designs for mangrove restoration. This assessment is done for a case study in Demak, Indonesia, using the numerical wave model SWASH. The empirical model of Gijon Mancheno et al. (2021) is used to estimate the bulk drag coefficient of the bamboo structures, and used as input for SWASH. Model results show good agreement with laboratory measurements that tested wave propagation through structures consisting of rows of cylinders. After the model validation, SWASH is applied in several design scenarios in order to find the optimum design. In these scenarios, three types of designs are considered: single row, double row and multiple rows. Three characteristic wave conditions are defined for Demak, ranging from daily conditions to extreme wave conditions, based on field measurements and WaveWatch III data. It is found that for the double-row design wave transmission rates stabilize for row separations longer than 20% of the significant wave length. For some of the longer distances, it is observed that the interaction of the transmitted and reflected waves between the rows slightly increases wave transmission due the formation of an anti-node at the first row.

Model results also suggest that structures with a separation of 20% of the wave length in wave direction may be optimal, and that at least 3 rows should be considered to achieve sufficient wave attenuation to induce sediment accretion behind the structures. Additional studies including morphodynamic assessments of the structures and the structural stability of the structures are recommended to optimize future bamboo structure designs.

Acknowledgements

The authors thank Han Winterwerp for the useful discussions about the practical considerations for Demak, Indonesia. We also like to thank Bas Hofland for the guidance in wave-structure interaction.

Author contributions

MA: Resources, Software, Writing-original draft; AGM: Supervision, Writing-review & editing; TS: Writing-review & editing ; AR: Supervision, Writing-review & editing.

Notations

Name	Symbol	Unit
Gravitational acceleration	g	m/s^2
Wave height	H	m
Wave period	T	s
Water depth	d	m
Wave length	L	m
Wave celerity	c	m/s
Wave group celerity	c_g	m/s
Wave number	k	1/m
Cross-shore location	x	m
Diameter	D	m
Along-shore location	y	m
Vertical location	z	m
Significant wave height	H_{m0}	m
Maximum wave height	H_{max}	m
Wave height exceed by 0.1 %	$H_{0.1\%}$	m
Bed shear stress	τ	N/m^2
Critical bed shear stress	τ_{crit}	N/m^2
Mass density of water	ρ_w	kg/m^3
Nominal diameter	d_{n50}	m
Ursell number	N_{Ur}	-
Keulegang - Carpenter number	KC	-
Reynolds number	Re	-
Return period	R	years
Flow velocity	u	m/s

References

- Abidin, H.Z., Andreas, H., Gumilar, I., Sidiq, T.P. and Fukuda, Y. (2013). Land subsidence in coastal city of Semarang (Indonesia): Characteristics, impacts and causes. *Geomatics, Natural Hazards and Risk*, 4(3), 226–240. ISSN 19475705. DOI:10.1080/19475705.2012.692336.
- Albers, T., Dinh Cong San and Schmitt, K. (2013). Coastal Protection in the Lower Mekong Delta. 124.
- Alferink, M. (2022). Wave transmission through permeable structures in Demak Indonesia.
- Balke, T., Bouma, T.J., Horstman, E.M., Webb, E.L., Erfteimeijer, P.L. and Herman, P.M. (2011). Windows of opportunity: Thresholds to mangrove seedling establishment on tidal flats. *Marine Ecology Progress Series*, 440, 1–9. ISSN 01718630. DOI:10.3354/meps09364.

- Bao, T.Q. (2011). Effect of mangrove forest structures on wave attenuation in coastal Vietnam. *Oceanologia*, **53**(3), 807–818. ISSN 00783234. DOI:10.5697/oc.53-3.807.
- Barbier, E.B., Hacker, S.D., Kennedy, C., Koch, E.W., Stier, A.C. and Silliman, B.R. (2011). The value of estuarine and coastal ecosystem services. *Ecological Monographs*, **81**(2), 169–193.
- Battjes, J.A. and Groenendijk, H.W. (2000). Wave height distributions on shallow foreshores. *Coastal Engineering*, **40**, 161–182. ISSN 03783839.
- Bonakdar, L., Oumeraci, H. and Etemad-Shahidi, A. (2015). Wave load formulae for prediction of wave-induced forces on a slender pile within pile groups. *Coastal Engineering*, **102**, 49–68. ISSN 03783839. DOI:10.1016/j.coastaleng.2015.05.003.
- Borsje, R.M. (2018). Assessing current patterns behind hybrid dams. 79.
- Borsje, R.M. (2019). Wave-Driven Set-Up of Fluid Mud. 100.
- Cao, H., Feng, W., Hu, Z., Suzuki, T. and Stive, M.J. (2015). Numerical modeling of vegetation-induced dissipation using an extended mild-slope equation. *Ocean Engineering*, **110**, 258–269. ISSN 00298018. DOI:10.1016/j.oceaneng.2015.09.057.
- Chen, Q. and Zhao, H. (2012). Theoretical Models for Wave Energy Dissipation Caused by Vegetation. *Journal of Engineering Mechanics*, **138**(2), 221–229. ISSN 0733-9399. DOI:10.1061/(asce)em.1943-7889.0000318.
- Dalrymple, B.R.a., Asce, M. and Kirby, J.T. (1984). Wave Diffraction Due To Areas. **110**(1), 67–79.
- Dalrymple, R.A. (1988). Scattering of long waves by cylindrical obstacles and gratings using matched asymptotic expansions. *Journal of Fluid Mechanics*, **188**, 465–490. ISSN 14697645. DOI:10.1017/S0022112088000801.
- Dao, H.T., Hofland, B., Suzuki, T., Stive, M.J.F., Mai, T. and Tuan, L.X. (2021). Numerical and small-scale physical modelling of wave transmission by wooden fences. **1**, 1–19.
- Dao, Tung, S.M.H.B.M.T. (2018). Wave Damping due to Wooden Fences along Mangrove Coasts. *Journal of Coastal Research*. DOI:https://doi.org/10.2112/JCOASTRES-D-18-00015.1.
- Dekkers, J.M. (2018). Undular bore development over coral reefs An experimental study.
- Etminan, V., Lowe, R.J. and Ghisalberti, M. (2019). Canopy resistance on oscillatory flows. *Coastal Engineering*, **152**(November). ISSN 03783839. DOI:10.1016/j.coastaleng.2019.04.014.
- Fenton, J.D. (1988). The numerical solution of steady water wave problems. *Computers and Geosciences*, **14**(3), 357–368. ISSN 00983004. DOI:10.1016/0098-3004(88)90066-0.
- Gijon Mancheno, A. (2022). *Restoring Mangroves with Structures*, Ph.D. thesis, Delft University of Technology.
- Gijon Mancheno, A., Jansen, W., Uijttewaal, W., Reniers, A., van Rooijen, A., Suzuki, T., Etminand, V. and Winterwerp, J. (2021). Wave transmission and drag coefficients through dense cylinder arrays: implications for designing structures for mangrove restoration. *Ecological Engineering*, (March, 2021). ISSN 0924-2244.
- Goda, Y. and Suzuki, Y. (1976). Estimation of incident and reflected waves in regular wave experiments. *Coastal Engineering*, **22**(1), 828–845. ISSN 00298018. DOI:10.1016/0029-8018(93)E0011-G.
- Guza, R.T. and Thornton, E.B. (1980). Local and shoaled comparisons of sea surface elevations, pressures, and velocities. *Journal of Geophysical Research*, **85**(C3), 1524. ISSN 0148-0227. DOI:10.1029/jc085ic03p01524.
- Hamilton, S.E. and Casey, D. (2016). Creation of a high spatio-temporal resolution global database of continuous mangrove forest cover for the 21st century (CGMFC-21). *Global Ecology and Biogeography*, **25**(6), 729–738. ISSN 14668238. DOI:10.1111/geb.12449.
- Holthuijsen, L.H. (2007). *Waves in Oceanic and Coastal waters*, Cambridge University Press.
- Hughes, S.A. (1993). Laboratory wave reflection analysis using co-located gages. *Coastal Engineering*, **20**(3-4), 223–247. ISSN 03783839. DOI:10.1016/0378-3839(93)90003-Q.
- Jansen, W.J. (2019). Wave dissipation in a permeable structure.

- Keulegan, G.H. and Carpenter, L.H. (1958). Forces on Cylinders and Plates in an Oscillating Fluid. *Journal of Research of the National Bureau of Standards*, **60**(75 -APMW-27). ISSN 04021215.
- Mai, T., Dao, T., Ngo, A. and Mai, C. (2020). Porosity effects on wave transmission through a bamboo fence. *APAC 2019 - Proceedings of the 10th International Conference on Asian and Pacific Coasts*, (Apac), 1413–1418. DOI:10.1007/978-981-15-0291-0_{_}191.
- Mai Van, C., Ngo, A., Mai, T. and Dao, H.T. (2021). Bamboo Fences as a Nature-Based Measure for Coastal Wetland Protection in Vietnam. *Frontiers in Marine Science*, **8**(October), 1–9. ISSN 22967745. DOI:10.3389/fmars.2021.756597.
- Massel, S.R., Furukawa, K. and Brinkman, R.M. (1999). Surface wave propagation in mangrove forests. *Fluid Dynamics Research*, **24**(4), 219–249. ISSN 01695983. DOI:10.1016/S0169-5983(98)00024-0.
- Maza, Maria, L.J.L.L.I.J. (2019). Experimental analysis of wave attenuation and drag forces in a realistic fringe rhizophora mangrove forest. *Advances in Water Resources*.
- McIvor, A., Spencer, T., Möller, I. and Spalding, M.D. (2013). The response of mangrove soil surface elevation to sea level rise Natural Coastal Protection Series: Report 3. *Natural Coastal Protection Series* ISSN, 2050–7941.
- Mendez, F.J. and Losada, I.J. (2004). An empirical model to estimate the propagation of random breaking and nonbreaking waves over vegetation fields. *Coastal Engineering*, **51**(2), 103–118. ISSN 03783839. DOI:10.1016/j.coastaleng.2003.11.003.
- Morison, J., Johnson, J. and Schaaf, S. (1950). The Force Exerted by Surface Waves on Piles. *Journal of Petroleum Technology*, **2**(05), 149–154. ISSN 0149-2136. DOI:10.2118/950149-g.
- Nepf, H.M. (1999). Drag, turbulence, and diffusion in flow through emergent vegetation. *Water Resources Research*, **35**(2), 479–489. ISSN 00431397. DOI:10.1029/1998WR900069.
- Phan Khanh, L. (2019). *Wave attenuation in coastal mangroves. Mangrove squeeze in the Mekong delta*.
- Quartel, S., Kroon, A., Augustinus, P.G., Van Santen, P. and Tri, N.H. (2007). Wave attenuation in coastal mangroves in the Red River Delta, Vietnam. *Journal of Asian Earth Sciences*, **29**(4), 576–584. ISSN 13679120. DOI:10.1016/j.jseaes.2006.05.008.
- Rees, F.V. (2019). Mangrove 's anchorage beyond opportunity. (August).
- Schmitt, K., Albers, T., Pham, T.T. and Dinh, S.C. (2013). Site-specific and integrated adaptation to climate change in the coastal mangrove zone of Soc Trang Province , Viet Nam. *Coastal conservation*, 545–558. DOI: 10.1007/s11852-013-0253-4.
- Sumer, B. Mutlu (Technical University of Denmark, D. and Fredsoe, Jorgen (Technical University of Denmark, D. (2006). *Hydrodynamics around cylindrical structures*, volume 26, World Scientific Publishing Co. Pte. Ltd., 5 Toh Tuck Link, Singapore 596224, revised ed edition.
- Suzuki, T., Hu, Z., Kumada, K., Phan, L.K. and Zijlema, M. (2019). Non-hydrostatic modeling of drag, inertia and porous effects in wave propagation over dense vegetation fields. *Coastal Engineering*, **149**(135), 49–64. ISSN 03783839. DOI:10.1016/j.coastaleng.2019.03.011.
- Suzuki, T., Zijlema, M., Burger, B., Meijer, M.C. and Narayan, S. (2012). Wave dissipation by vegetation with layer schematization in SWAN. *Coastal Engineering*, **59**(1), 64–71. ISSN 03783839. DOI:10.1016/j.coastaleng.2011.07.006.
- Swart, D. (1976). Predictive equations regarding coastal transport. *Proc. 15th Conf. Coastal Eng.*
- Tas, S.A., van Maren, D.S. and Reniers, A.J. (2020). Observations of cross-shore chenier dynamics in Demak, Indonesia. *Journal of Marine Science and Engineering*, **8**(12), 1–18. ISSN 20771312. DOI:10.3390/jmse8120972.
- The United Nations, F..A.O. (2003). New global estimate of mangroves.
- Tonneijck, F., Van der Goot, F. and Pearce, F. (2022). Building with Nature in Indonesia. Restoring an eroding coastline and inspiring action at scale. *Wetlands International and Ecoshape Foundation*.
- Tonneijck, F., Winterwerp, H., Weesenbeeck, B.v., Bosma, R., Debrot, D., Noor, Y.R. and Wilms, T. (2015). Building with Nature Indonesia Securing Eroding Delta Coastlines. 1–65.

Van Domburg, T., Smits, I.B.P. and Van Bijsterveldt, C.E.J. (2018). Identifying Windows of Opportunity for Mangrove Establishment on a Mud Coast.

van Rooijen, A., Lowe, R., Rijnsdorp, D.P., Ghisalberti, M., Jacobsen, N.G. and McCall, R. (2020). Wave-Driven Mean Flow Dynamics in Submerged Canopies. *Journal of Geophysical Research: Oceans*, **125**(3), 1–21. ISSN 21699291. DOI:10.1029/2019JC015935.

van Rooijen, A.A., McCall, R.T., van Thiel de Vries, J.S., van Dongeren, A.R., Reniers, A.J. and Roelvink, J.A. (2016). Modeling the effect of wave-vegetation interaction on wave setup. *Journal of Geophysical Research: Oceans*, **121**(6), 4341–4359. ISSN 21699291. DOI:10.1002/2015JC011392.

Winterwerp, J.C., Albers, T., Anthony, E.J., Friess, D.A., Mancheño, A.G., Moseley, K., Muhari, A., Naipal, S., Noordermeer, J., Oost, A., Saengsupavanich, C., Tas, S.A., Tonneijck, F.H., Wilms, T., Van Bijsterveldt, C., Van Eijk, P., Van Laveren, E. and Van Wesenbeeck, B.K. (2020). Managing erosion of mangrove-mud coasts with permeable dams – lessons learned. *Ecological Engineering*, **158**(June), 106078. ISSN 09258574. DOI:10.1016/j.ecoleng.2020.106078.

Winterwerp, J.C., Borst, W.G. and De Vries, M.B. (2005). Pilot study on the erosion and rehabilitation of a mangrove mud coast. *Journal of Coastal Research*, **21**(2), 223–230. ISSN 07490208. DOI:10.2112/03-832A.1.

Yin, K., Xu, S., Huang, W., Liu, S. and Li, M. (2021). Numerical investigation of wave attenuation by coupled flexible vegetation dynamic model and XBeach wave model. *Ocean Engineering*, **235**(June). ISSN 00298018. DOI: 10.1016/j.oceaneng.2021.109357.

A Grid-size dependence

The assumption of uniform placement of poles means that the pole to pole distance in x and y direction is the same. However, in the longitudinal configuration, shown in Figure 3, the pole to pole distance in x direction is larger (12 cm) compared to the one in y-direction (6 cm), and thus it is not uniform. To make this uniform though, requires adjusting the dx grid size. Keeping in mind that each individual row is specified in the grid of the configuration, it is therefore needed to match the width of the row with the pole to pole distance in y direction. With a dx of 3 cm and a diameter of the poles of 4 cm, this gives a row width of 6 cm, as 2 points are needed. In these simulations a x-y grid is not used, but a x-z grid, nonetheless, this has never been examined and may be important for using the vegetation module as design tool.

To investigate this the two setups are compared, where the main changes are the change in dx and as the row width changes the number of cylinders per m^2 also changes. It was already found which method of mass conservation works best per configuration so those parameters are kept the same.

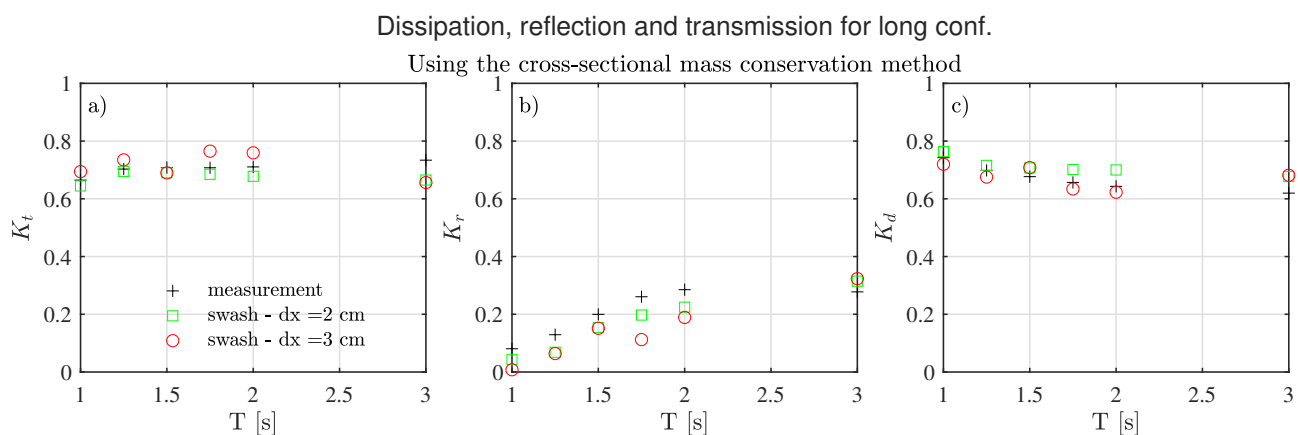


Figure 16: Results of the longitudinal configuration, sensitivity to change in grid size. With from left to right: transmission, reflection and dissipation in the form of $K_{t,r,d} = H_{t,r,d}/H_i$. On the x-axis are the wave periods belonging with wave conditions in Table 1. This configuration is not so sensitive to changes in the grid size.

In Figure 16 it is observed that the case with $dx = 3$ cm, has slightly lower dissipation values and therefore higher transmission rates but both setups follow the same pattern and hardly differ. As this configuration proves to be insensitive to changes in the grid size, in the design phase the required grid size is not so strictly limited anymore as long as the density and row width are accurately described.

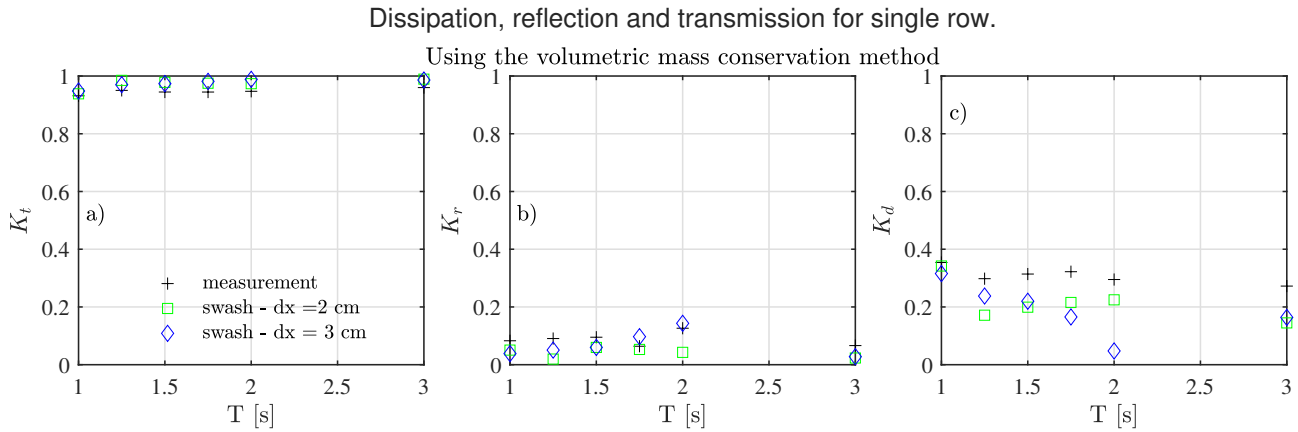


Figure 17: Results of the single row configuration, sensitivity to change in grid size. With from left to right: transmission, reflection and dissipation in the form of $K_{t,r,d} = H_{t,r,d}/H_i$. On the x-axis are the wave periods belonging with wave conditions in Table 1. This configuration is more sensitive to changes in the grid size than the longitudinal configuration.

In Figure 17 is observed that the case with $dx = 2$ cm shows a modest improvement compared with the measured dissipation rates, whereas for reflection and transmission the rates are similar between the two setups.

B Bulk drag coefficients

Table 8: Bulk drag coefficient for each s_x distance per wave condition

s_x	3 D	4 D	5 D	6 D	7 D	8 D	9 D	10 D
s_x [m]	0.42	0.56	0.70	0.84	0.98	1.12	1.26	1.4
$C_{d,b}$ (R = 1 & 5 yr)	3.30	4.28	4.95	5.43	5.79	6.08	6.30	6.49
$C_{d,b}$ (Daily cond.)	3.75	4.86	5.63	6.18	6.59	6.91	7.17	7.38
s_x	$L_{rp1}/20$	$L_{rp1}/15$	$L_{rp1}/10$	$L_{rp1}/8$	$L_{rp1}/6$	$L_{rp1}/5$	$L_{rp1}/4$	$L_{rp1}/3$
s_x [m]	1.45	1.90	2.90	3.50	4.70	5.80	7.30	9.70
$C_{d,b}$ (R = 1 & 5 yr)	6.49	6.92	7.37	7.55	7.74	7.85	7.94	8.04
$C_{d,b}$ (Daily cond.)	7.38	7.87	8.38	8.59	8.80	8.93	9.04	9.14
s_x	$L_{rp1}/2$	$\frac{2}{3}L_{rp1}$	$\frac{3}{4}L_{rp1}$	L_{rp1}				
s_x [m]	14.5	19.3	21.80	29.0				
$C_{d,b}$ (R = 1 & 5 yr)	8.13	8.18	8.19	8.23				
$C_{d,b}$ (Daily cond.)	9.25	9.30	9.32	9.36				

C Reflections

Figure 18 describes the reflection rates of the double row design. It can be noticed that for the wave conditions with an one year return period that these are also influenced, in lesser scale, by the separation length (s_x) as the transmission rates in Figure 11 b, best noticeable with the relative high values around $0.5 s_x/L$ and the relative low values around 0.35 and $0.75 s_x/L$. The high values correspond to high transmission rates.

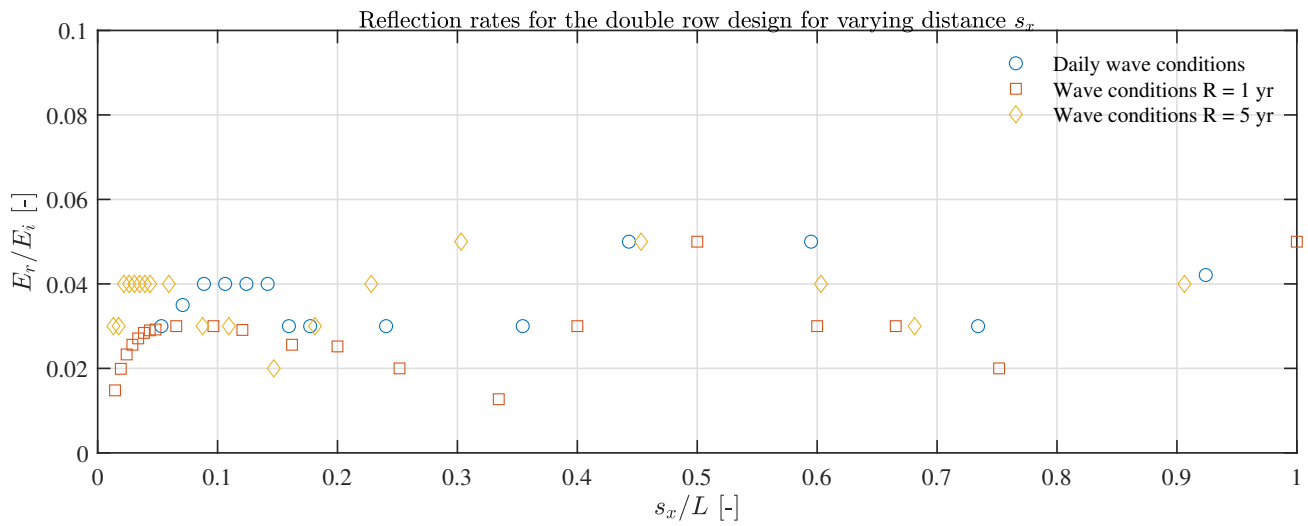


Figure 18: Reflection rates for the double row design for the three waves conditions. Maximum reflection rates do not exceed 6%.